Available online at www.sciencedirect.com
ScienceDirect
Ceramics International 38S (2012) S327–S330
CERAMICS INTERNATIONAL
www.elsevier.com/locate/ceramint

Relationships between crystal structure and electrical properties of $Li_{0.055}[Ag_x(K_{0.5}Na_{0.5})_{1-x}]_{0.945}(Nb_{1-y}Ta_y)O_3$ ceramics

Seock No Seo [a], Jeong Ho Cho [b], Byung Ik Kim [b], Eung Soo Kim [a,*]

[a] Department of Materials Engineering, Kyonggi University, Suwon 443-760, Republic of Korea
[b] Korea Institute of Ceramic Engineering and Technology, Seoul 153-801, Republic of Korea

Available online 4 May 2011

Abstract

Electrical properties of perovskite $Li_{0.055}[Ag_x(K_{0.5}Na_{0.5})_{1-x}]_{0.945}(Nb_{1-y}Ta_y)O_3$ ($0.00 \le x \le 0.04$, $0.01 \le y \le 0.09$) ceramics were investigated based on the structural characteristics. A morphotropic phase boundary (MPB) between orthorhombic and tetragonal phase was detected through the entire range of compositions. With increasing of Ta^{5+} content, the dielectric constant (ε_r), piezoelectric coefficient (d_{33}) and electromechanical coupling factor (k_p) of $Li_{0.055}(K_{0.5}Na_{0.5})_{0.945}(Nb_{1-y}Ta_y)O_3$ ceramics were increased up to $y = 0.07$ and then decreased, while mechanical quality factor (Q_m) was increased. However, the ε_r, d_{33}, k_p and Q_m of $Li_{0.055}[Ag_x(K_{0.5}Na_{0.5})_{1-x}]_{0.945}(Nb_{0.07}Ta_{0.03})O_3$ ceramics were not changed remarkably with Ag^+ content. The dependence of temperature coefficient of k_p (TCk_p) on the oxygen octahedral distortion was also discussed by Raman-active vibrations modes.

Keywords: A. Sintering; C. Electric properties; D. Perovskites; (K, Na)NbO_3

1. Introduction

For lead-free piezoelectric materials $(K_{0.5}Na_{0.5})NbO_3$ (KNN)-based ceramics were widely investigated to improve their electrical properties with preparing compositions close to morphotropic phase boundary (MPB) and shifting the orthorhombic–tetragonal (*O–T*) phase transition to near or below room temperature. Although these ceramics show the good electrical properties at room temperature, the temperature stability of the electrical properties is relatively poor which obstruct for practical applications [1]. Therefore, the thermal stability of KNN ceramics should be considered from the point view of practical applications.

Also, several types of KNN-based ceramics such as KNN-$LiNbO_3$ [2], KNN-$LiTaO_3$ [3] and KNN-$AgNbO_3$ [4] have been reported to improve the sintering behavior of KNN ceramics as well as the shift of *O–T* phase transition to near or below room temperature. However, most recent studies in this field have been focused on the development of KNN-based ceramics with the enhancement of piezoelectric properties through doping or texture control.

Since the electrical properties of KNN-based ceramics with perovskite structure could be affected by the structural characteristics such as oxygen octahedral distortion resulting from the difference of bond length and strength between cation and oxygen ion of the unit cell, the dependence of electrical properties on the structural characteristics of KNN-based ceramics should be studied in detail which is available to predict and control the electrical properties of KNN-based ceramics.

The substitution of cations with different ionic sizes and/or electronegativity for A and/or B-site ions in ABO_3 perovskite structure could induce the change of the volume fraction of orthorhombic and tetragonal phases in the MPB region, which affect the electrical properties of the KNN-based ceramics.

Based on these considerations, the electrical properties of $Li_{0.055}[Ag_x(K_{0.5}Na_{0.5})_{1-x}]_{0.945}(Nb_{1-y}Ta_y)O_3$ ceramics were investigated as a function of Ag^+ and/or Ta^{5+} content in this study. The dependences of the temperature coefficient of electromechanical coupling factor (TCk_p) on the average distortion of oxygen octahedra with orthorhombic and tetragonal phases were also discussed for thermal stability.

* Corresponding author. Tel.: +82 31 249 9764; fax: +82 31 244 6300.
E-mail address: eskim@kyonggi.ac.kr (E.S. Kim).

0272-8842/$36.00
doi:10.1016/j.ceramint.2011.04.112

2. Experimental procedures

$Li_{0.055}[Ag_x(K_{0.5}Na_{0.5})_{1-x}]_{0.945}(Nb_{1-y}Ta_y)O_3$ (LKNNT ($x = 0.00$, $0.01 \leq y \leq 0.09$), LAKNNT ($0.00 \leq x \leq 0.04$, $y = 0.03$)) were prepared by the conventional solid-state reaction from oxide powders with purities above 99.9%. Mixed powders of the desired compositions calcined at 850 °C for 5 h were milled again with ZrO_2 balls for 24 h in ethanol and then dried. The dried powders were pressed isostatically into 10 mm-diameter disks at 1500 kg/cm^2. These pellets were sintered at 1100 °C for 5 h in air.

Powder X-ray diffraction (XRD, D/Max-3C, Rigaku, Japan) analysis was used to identify the crystalline phases of the sintered specimens. The lattice parameters, unit-cell volumes and atomic positions were obtained by Rietveld refinements of XRD patterns using Fullprof [5]. The initial structure model for $(K_{0.5}Na_{0.5})NbO_3$ compounds was taken from the previous reports [6,7]. During the first stage of the refinement, zero shift, individual scale factor and unit-cell parameters were only the refined parameters until an apparent convergence was reached. And then, the phase profile parameters (U, V and W) and two asymmetry parameters were included until final convergence. The change of bond length was confirmed by a Raman spectra meter (T 64000, HORIABA Jobin Yvon, France) with an Ar^+ ion laser operating at 514 nm for excitation.

Silver electrodes were formed on both surfaces of each sintered disk by firing at 700 °C for 10 min. The samples were polarized in silicon oil bath at 120 °C by applying a DC electric field (4–5 kV mm^{-1} for 20 min). The dielectric constant was measured as a function of temperature by LCR meter (HP 4284A, Agilent, USA). The piezoelectric coefficient (d_{33}) was measured using a piezo-d_{33} meter (ZJ-3BN, Institute of Acoustics, Chinese Academy of Sciences, China). The electromechanical coupling coefficient (k_p) and mechanical quality factor (Q_m) were determined by the resonance and anti-resonance method on the basis of IEEE standards using an impedance analyzer (HP 4192A, Palo Alto, CA, USA). Microstructure of the specimens was observed using a scanning electron microscope (SEM, JSM-6500F, JEOL, Japan).

3. Results and discussion

For the specimens of $Li_{0.055}[Ag_x(K_{0.5}Na_{0.5})_{1-x}]_{0.945}(Nb_{1-y}Ta_y)O_3$ (LKNNT ($x = 0.00$, $0.01 \leq y \leq 0.09$), LAKNNT ($0.00 \leq x \leq 0.04$, $y = 0.03$)) at sintered at 1100 °C for 5 h, the relative densities of the specimens were above 94% and all of the specimens did not show any deliquescent. Fig. 1 shows the XRD patterns of LKNNT and/or LAKNNT specimens sintered at 1100 °C for 5 h. A single phase of perovskite structure was detected through the entire range of compositions. The morphotropic phase boundary (MPB) between the orthorhombic (*Amm*2) and tetragonal (*P*4*mm*) phase was confirmed from $2\theta = 44°$ to $2\theta = 47°$. Comparing to the peak of orthorhombic phase (0 0 2), the peak of tetragonal phase (2 2 0) was increased continuously with increasing of Ag^+ and/or Ta^{5+} content. However, the change of (0 0 2) peak with Ta^{5+} content was larger than that with Ag^+ content.

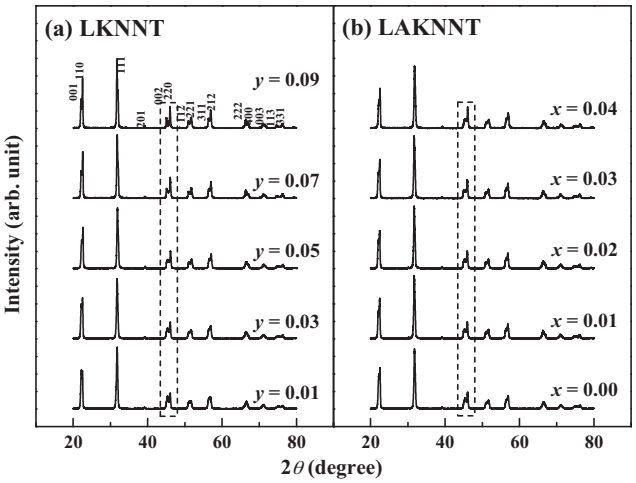

Fig. 1. XRD patterns of $Li_{0.055}[Ag_x(K_{0.5}Na_{0.5})_{1-x}]_{0.945}(Nb_{1-y}Ta_y)O_3$ specimens sintered at 1100 °C for 5 h; (a) LKNNT ($x = 0.00$, $0.01 \leq y \leq 0.09$), (b) LAKNNT ($0.00 \leq x \leq 0.04$, $y = 0.03$).

For the analysis of structural characteristics in MPB region, the Rietveld refinement procedures was performed on two types of the initial structure mode of the orthorhombic (ICSD # 18502) and tetragonal (ICSD # 2855) at the same time. The bond lengths, unit-cell volume and volume fraction of each space group obtained from Rietveld refinement are shown in Table 1. With increasing of Ag^+ and/or Ta^{5+} content, the volume fraction of orthorhombic (*Amm*2) phase was decreased, while that of tetragonal (*P*4*mm*) phase was increased. Also, the lattice parameters and unit-cell volume of the specimens were changed with Ag^+ and/or Ta^{5+} content. These results could be attributed to the differences of bond strength and length between the composing ions of compound by solid solution of Ag^+ and/or Ta^{5+} ion, which could be confirmed by the Raman-active vibrations.

Fig. 2 shows the Raman spectrum of the sintered specimens. A_{1g} and F_{2g} modes indicate the double degenerate symmetric O–Nb–O stretching vibration and the triply degenerate symmetric O–Nb–O bending vibration, respectively [8]. A_{1g} and F_{2g} modes of the specimens move to higher wavenumber with Ta^{5+} content, while those of the specimens were not changed remarkably with Ag^+ content. The shift of Raman modes to higher wavenumber means the increase of the bond strengths between Nb^{5+} and its coordinated oxygen, which induce the distortion of crystal structure. These results could be attributed to the distortion of O–Nb–O angles of B-site oxygen octahedra by the substitution of B-site than A-site of ABO_3 perovskite structure. For the NbO_6 octahedra, the bond lengths of specimens with space group of *Amm*2 (orthorhombic) showed the four types of $2 \times d_1$, $2 \times d_2$, $1 \times d_3$, and $1 \times d_4$ while those of specimens with space group of *P*4*mm* (tetragonal) showed the three types of $1 \times d_1$, $1 \times d_2$ and $4 \times d_3$ (Table 1).

These changes of bond lengths affect the distortion of NbO_6 octahedra which is calculated by Eq. (1) [9].

$$\Delta = \left(\frac{1}{6}\right) \sum \frac{R_i - \bar{R}^2}{\bar{R}^2} \quad (1)$$

Table 1
Crystallographic data and refinement statistics obtained from a Rietveld refinement for $Li_{0.055}[Ag_x(K_{0.5}Na_{0.5})_{1-x}]_{0.945}(Nb_{1-y}Ta_y)O_3$ ($0.00 \le x \le 0.04$, $0.01 \le y \le 0.09$) specimens sintered at 1100 °C for 5 h.

x (mol)	y (mol)	Space group	Bond length (Å)				$V_{unit\text{-}cell}$ (Å^3)	[a]V.F.	[b]R_B (%)
			d_1	d_2	d_3	d_4			
0.01	0.03	*Amm*2	2.190	1.840	1.896	2.101	125.33	0.52	6.63
		*P*4*mm*	2.167	1.852	1.978	–	62.46	0.48	7.82
0.02	0.03	*Amm*2	2.187	1.859	1.884	2.118	125.26	0.50	5.84
		*P*4*mm*	2.167	1.852	1.978	–	62.47	0.50	7.13
0.03	0.03	*Amm*2	2.190	1.840	1.893	2.097	125.30	0.43	5.83
		*P*4*mm*	2.167	1.852	1.978	–	62.46	0.57	7.47
0.04	0.03	*Amm*2	2.179	1.854	1.886	2.115	125.25	0.40	6.13
		*P*4*mm*	1.978	1.851	1.978	–	62.41	0.60	8.20
0.00	0.01	*Amm*2	2.191	1.841	1.895	2.099	125.36	0.70	5.53
		*P*4*mm*	2.168	1.853	1.979	–	65.52	0.30	5.67
0.00	0.03	*Amm*2	2.165	1.905	1.807	2.183	125.25	0.56	7.03
		*P*4*mm*	2.167	1.852	1.979	–	62.49	0.44	7.59
0.00	0.05	*Amm*2	2.193	1.837	1.860	2.132	125.41	0.34	8.11
		*P*4*mm*	2.167	1.852	1.979	–	62.51	0.66	8.42
0.00	0.07	*Amm*2	2.202	1.847	1.877	2.136	125.33	0.20	8.60
		*P*4*mm*	2.167	1.852	1.979	–	62.47	0.80	9.25
0.00	0.09	*Amm*2	2.189	1.836	1.896	2.101	125.00	0.10	10.1
		*P*4*mm*	2.167	1.852	1.978	–	62.28	0.90	8.60

[a] Volume fraction.
[b] Bragg *R*-factor.

where R_i is the individual bond length, and $\bar{R}$ is average bond length of oxygen octahedra, respectively. The octahedral distortion of the specimens with space group of *Amm*2 (orthorhombic) was much larger than that of the specimens with space group of *P*4*mm* (tetragonal) due to the difference of bond types of oxygen octahedra. Therefore, the average octahedral distortion of the specimens was calculated from the volume fraction of each phase. The average octahedral distortion of the specimens was decreased with Ag^+ and/or Ta^{5+} content due to the increase of volume fraction of tetragonal (*P*4*mm*) phase which has smaller types of bond length than orthorhombic (*Amm*2) phase. However, the average octahedral distortion of the specimens with Ta^{5+} content was more largely decreased than that of the specimens with Ag^+ content. These results could be attributed to the difference of bond length between cation and oxygen ion.

To investigate the thermal stability of the ceramics, the temperature coefficient of electromechanical coupling factor (TCk_p) from 30 °C to 80 °C is calculated from Eq. (2) [10].

$$TCk_p = \frac{k_{p,80\,^\circ\mathrm{C}} - k_{p,30\,^\circ\mathrm{C}}}{k_{p,30\,^\circ\mathrm{C}}} \quad (2)$$

Fig. 3 shows the dependence of TCk_p on the average oxygen octahedral distortion for the sintered specimens. The TCk_p of the specimens was decreased with Ag^+ and/or Ta^{5+} content due to the decrease of average octahedral distortion.

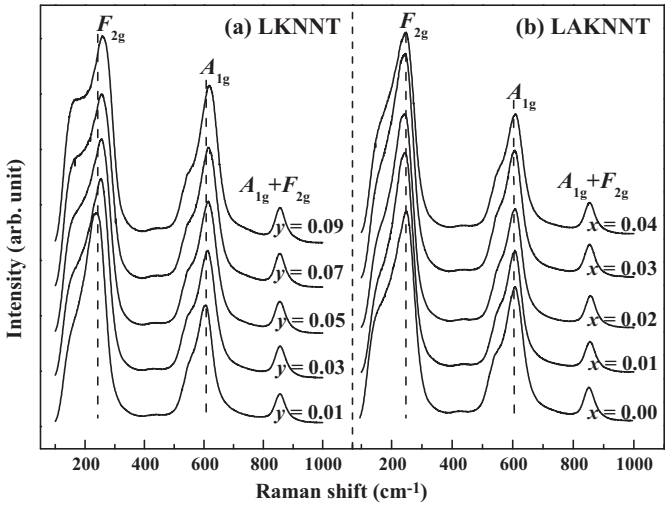

Fig. 2. Raman spectrum of $Li_{0.055}[Ag_x(K_{0.5}Na_{0.5})_{1-x}]_{0.945}(Nb_{1-y}Ta_y)O_3$ specimens sintered at 1100 °C for 5 h; (a) LKNNT ($x = 0.00$, $0.01 \le y \le 0.09$), (b) LAKNNT ($0.00 \le x \le 0.04$, $y = 0.03$).

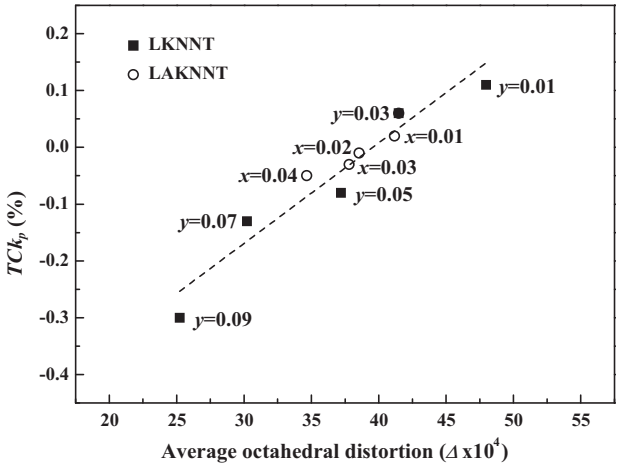

Fig. 3. Dependence of TCk_p on the average oxygen octahedral distortion for $Li_{0.055}[Ag_x(K_{0.5}Na_{0.5})_{1-x}]_{0.945}(Nb_{1-y}Ta_y)O_3$ specimens sintered at 1100 °C for 5 h; LKNNT ($x = 0.00$, $0.01 \le y \le 0.09$), LAKNNT ($0.00 \le x \le 0.04$, $y = 0.03$).

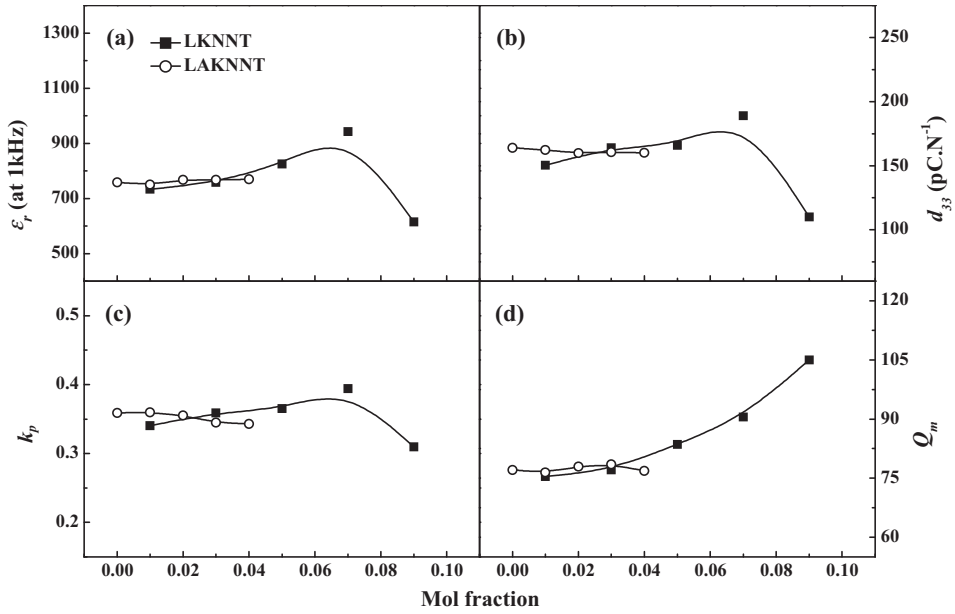

Fig. 4. Electrical properties ((a) ε_r, (b) d_{33}, (c) k_p and (d) Q_m) of $Li_{0.055}[Ag_x(K_{0.5}Na_{0.5})_{1-x}]_{0.945}(Nb_{1-y}Ta_y)O_3$ specimens sintered at 1100 °C for 5 h; LKNNT ($x = 0.00$, $0.01 \leq y \leq 0.09$), LAKNNT ($0.00 \leq x \leq 0.04$, $y = 0.03$).

The dielectric constant (ε_r), piezoelectric coefficient (d_{33}), electromechanical coupling factor (k_p) and mechanical quality factor (Q_m) of the sintered specimens are shown in Fig. 4. The ε_r, d_{33}, k_p and Q_m of the specimens with Ag^+ showed nearly a constant value through the range of entire compositions. For the specimens with Ta^{5+}, although the Q_m was increased with Ta^{5+} content due to the increase of relative density, the ε_r, d_{33} and k_p were slightly increased up to $y = 0.07$ and then drastically decreased. These results could be explained that the specimens with $y = 0.09$ were mainly composed of tetragonal phase ($P4mm$), which in turn, the domain wall of the specimens could not easily move beyond MPB region.

From the SEM micrographs (not shown), the grain size of the specimens was slightly decreased with Ta^{5+} content, while that of the specimens was not changed with Ag^+ content. Therefore, the effects of gain size on the mechanical quality factor (Q_m) could be neglected.

4. Conclusions

For the specimens of $Li_{0.055}[Ag_x(K_{0.5}Na_{0.5})_{1-x}]_{0.945}(Nb_{1-y}Ta_y)O_3$ ($0.00 \leq x \leq 0.04$, $0.01 \leq y \leq 0.09$) sintered at 1100 °C for 5 h, the morphotropic phase boundary (MPB) between orthorhombic ($Amm2$) and tetragonal ($P4mm$) phase was detected through the entire range of compositions.

With increasing of Ag^+ and/or Ta^{5+} content, the temperature coefficient of k_p (TCk_p) of the specimens was decreased due to the decrease of average oxygen octahedral distortion by Raman shift of A_{1g} and F_{2g} mode. Even though the electrical properties (ε_r, d_{33}, k_p and Q_m) of $Li_{0.055}[Ag_x(K_{0.5}Na_{0.5})_{1-x}]_{0.945}$ $(Nb_{0.07}Ta_{0.03})O_3$ ceramics were not changed remarkably with Ag^+ content, the ε_r, d_{33} and k_p of $Li_{0.055}(K_{0.5}Na_{0.5})_{0.945}$ $(Nb_{1-y}Ta_y)O_3$ ceramics were increased with Ta^{5+} content up to $y = 0.07$ and then decreased, while the Q_m of the specimens was increased.

Acknowledgement

This research was supported by a grant from the Fundamental R&D Program for Core Technology of Materials funded by the Ministry of Knowledge Economy, Republic of Korea.

References

[1] E. Hollenstein, D. Damjanovic, N. Setter, Temperature stability of the piezoelectric properties of Li-modified KNN ceramics, Journal of the European Ceramic Society 27 (2007) 4093–4097.
[2] Y. Wang, J. Wu, D. Xiao, J. Zhu, P. Yu, L. Wu, X. Li, Piezoelectric properties of (Li, Ag) modified $(Na_{0.50}K_{0.50})NbO_3$ lead-free ceramics with high Curie temperature, Journal of Alloys and Compounds 459 (2008) 414–417.
[3] Y. Guo, K. Kakimoto, H. Ohsato, $(Na_{0.5}K_{0.5})NbO_3$-$LiTaO_3$ lead-free piezoelectric ceramics, Materials Letters 59 (2005) 241–244.
[4] C. Lei, Z.G. Ye, Lead-free piezoelectric ceramics derived from the $K_{0.5}Na_{0.5}NbO_3$–$AgNbO_3$ solid solution system, Applied Physics Letters 93 (2008) 042901.
[5] T. Roisnel, J.R. Carvajal, WinPLOTR: a windows tool for powder diffraction patterns analysis, Materials Science Forum 378–381 (2001) 118–123.
[6] V.A. Shuvaeva, M.Y. Antipin, Structural disorder in $KNbO_3$ crystal from X-ray diffraction and EXAFS spectroscopy, Kristallografiya 40 (1995) 511–516.
[7] A.W. Hewat, Soft modes and the structure, spontaneous polarization and Curie constants of perovskite ferroelectrics: tetragonal potassium niobate, Journal of Physics C: Solid State Physics 6 (1973) 1074–1084.
[8] H.R Xia, H.C. Chen, H. Yu, K.X. Wang, B.Y. Zhao, Vibrational spectra of a $K_{0.30}Na_{0.10}Sr_{0.48}Ba_{0.32}Nb_2O_6$ single crystal studied by Raman and infrared reflectivity spectroscopy, Physica Status Solidi B 210 (1998) 47–59.
[9] R.D. Shannon, Revised effective ionic radii and systematic studies of interatomic distances in halides and chalcogenides, Acta Crystallographica A 32 (1976) 751–767.
[10] L. Wu, D. Xiao, J. Wu, Y. Sun, D. Lin, J. Zhu, P. Yu, Y. Zhuang, Q. Wei, Good temperature stability of $K_{0.5}Na_{0.5}NbO_3$ based lead-free ceramics and their applications in buzzers, Journal of the European Ceramic Society 28 (2008) 2963–2968.